The E⊗e dynamic Jahn-Teller problem: A new insight from the strong coupling limit

AUTHOR(S):

Sato, Tohru; Chibotaru, Liviu F.; Ceulemans, Arnout

THE JOURNAL OF CHEMICAL PHYSICS **122**, 054104 (2005)

The $E\otimes e$ dynamic Jahn-Teller problem: A new insight from the strong coupling limit

Tohru Sato[a)]
Division of Quantum Chemistry, Catholic University of Leuven, Celestijnenlaan 200F, B-3001 Leuven, Belgium; Fukui Institute for Fundamental Chemistry, Kyoto University, Takano-Nishihiraki-cho 34-4, Sakyo-ku, Kyoto 606-8103, Japan; and Department of Molecular Engineering, School of Engineering, Kyoto University, Kyoto 615-8510, Japan

Liviu F. Chibotaru and Arnout Ceulemans
Division of Quantum Chemistry, Catholic University of Leuven, Celestijnenlaan 200F, B-3001 Leuven, Belgium

(Received 6 October 2004; accepted 1 November 2004; published online 14 January 2005)

Correct boundary conditions for the $E\otimes e$ dynamic Jahn-Teller problem are considered explicitly for the first time to obtain approximate analytical solutions in the strong coupling limit. Numerical solutions for the decoupled equations using the finite difference method are also presented. The numerical solutions for the decoupled equations exhibit avoided crossings in the weak coupling region, which explains the oscillating behavior of the solutions obtained by Longuet-Higgins *et al.* for the coupled equations. The obtained analytical energy expressions show improved agreement with the numerical calculations as compared with the previous treatment in which the potentials were assumed to be harmonic. We demonstrate that the pseudorotational energy $j^2/(2g^2)$, where g is the dimensionless vibronic coupling constant, and j total angular momentum: $j=\pm 1/2, \pm 3/2,\ldots$, in the conventional strong coupling expression for the vibronic levels of the lower sheet is exact. Non-Hermitian first-order perturbation theory gives the energy which is correct up to $1/g^4$. The asymptotic behavior of the wave function at the origin does not influence the corrected energy up to order of $1/g^4$. At the same time the treatment of the upper sheet with correct boundary conditions gives solutions which are entirely different from the corresponding Slonczewski's solutions. Besides, the correct boundary conditions enable us to evaluate the nonadiabatic coupling between the lower and upper potential sheets. The energy correction due to the nonadiabatic coupling is estimated to be of order $1/g^6$. © *2005 American Institute of Physics.*
[DOI: 10.1063/1.1836758]

I. INTRODUCTION

The *dynamical Jahn-Teller* (JT) *problem* is one of the most investigated problems in molecular physics. However, the analytical solution in the general case has not been established.

The first numerical calculations for the energy spectra of the dynamic $E\otimes e$ JT problem describing the coupling of a twofold degenerate electronic E state with a twofold degenerate vibrational e state, were performed more than 40 years ago.[1,2] Since then, many authors have studied this problem numerically.[3,4] On the other hand, first progress towards the exact solution was made by Judd.[5] He obtained finite-order equations for the isolated values of the coupling constant in which the eigenvalue lies on a baseline. Efforts to obtain analytical solutions are continuing even today.[6–10]

The dynamic linear $E\otimes e$ JT problem in the strong coupling limit has been investigated since 1958.[1,11,12] These solutions in the strong coupling limit are called the crude solutions in the present paper. The crude solution which is obtained assuming a harmonic potential can reproduce the numerical calculation well in the strong coupling limit up to order of $1/g^2$, where g is dimensionless vibronic coupling constant. However, the radial wave function within the crude approximation does not satisfy the boundary condition at the origin and gives rise to divergent nonadiabatic coupling elements. A similar problem that singularity appears in the Hamiltonian based on the diabatic representation has also been discussed.[13–15]

In this paper, we will present a simple approximate analytical solution which satisfies the correct boundary condition at the origin for the dynamical linear $E\otimes e$ problem in the strong coupling limit. First-order perturbation is employed to obtain up to $1/g^4$ contribution. The whole treatment for the lower energy surface demonstrates the existence of the pseudorotational energy $j^2/(2g^2)$ in the vibronic spectra in the strong coupling limit. We will also present the nonadiabatic coupling matrix elements using the obtained solutions.

The paper is organized as follows: In Sec. II we formulate the $E\otimes e$ Jahn-Teller Hamiltonian in the adiabatic basis and decouple the equations in the strong coupling limit. In Sec. III we show the numerical solution of the decoupled equation using the finite difference method and compare it with the exact numerical solution of the coupled equations obtained by Longuet-Higgins *et al.* The solutions within the

a)Electronic mail: tsato@scl.kyoto-u.ac.jp

crude approximation are presented in Sec. IV. In Sec. V, we consider the asymptotic behavior in the vicinity of the origin which the solutions of the coupled and decoupled equation should satisfy. The approximate analytical solution of the decoupled equation for the lower sheet is presented in Sec. VI. In Sec. VII, first-order perturbation for the solution is calculated to obtain the energy correction up to $1/g^4$ order. The solution for the upper sheet is presented in Sec. VIII. In Sec. IX, the nonadiabatic coupling is evaluated.

II. $E\otimes e$ DYNAMIC JAHN-TELLER HAMILTONIAN

The Hamiltonian for the linear $E\otimes e$ dynamic Jahn-Teller problem is written within the space spanned by complex electronic states $\psi_\pm = 1/\sqrt{2}(\phi_\theta \pm i\phi_\epsilon)$ as

$$\hat{\mathcal{H}} = -\frac{1}{2}\left\{\left(\frac{\partial^2}{\partial Q_\theta^2}+\frac{\partial^2}{\partial Q_\epsilon^2}\right)-(Q_\theta^2+Q_\epsilon^2)\right\}\hat{\sigma}_0 + g(Q_\theta\hat{\sigma}_x + Q_\epsilon\hat{\sigma}_y), \tag{1}$$

where g is a dimensionless vibronic coupling constant and (Q_θ, Q_ϵ) are real normal coordinates of an e vibrational mode, and

$$\hat{\sigma}_0 = \begin{pmatrix} 1 & 0 \\ 0 & 1 \end{pmatrix}, \quad \hat{\sigma}_x = \begin{pmatrix} 0 & 1 \\ 1 & 0 \end{pmatrix}, \quad \hat{\sigma}_y = \begin{pmatrix} 0 & -i \\ i & 0 \end{pmatrix}. \tag{2}$$

Throughout this article, energy is measured by $\hbar\omega$, length as $\sqrt{\hbar/(m\omega)}$, and momentum as $\sqrt{m\omega\hbar}$ to obtain dimensionless quantities. If (Q_θ, Q_ϵ) are written in polar coordinates,

$$Q_\theta = \rho\cos\phi,$$

$$Q_\epsilon = \rho\sin\phi,$$

the vibronic interaction matrix can be written as[12]

$$g(Q_\theta\hat{\sigma}_x + Q_\epsilon\hat{\sigma}_y) = g\rho\begin{pmatrix} 0 & e^{-i\phi} \\ e^{i\phi} & 0 \end{pmatrix}. \tag{3}$$

Therefore the Hamiltonian in polar coordinates is given by

$$\hat{\mathcal{H}} = \left[-\frac{1}{2}\left\{\frac{1}{\rho}\frac{\partial}{\partial\rho}\left(\rho\frac{\partial}{\partial\rho}\right)+\frac{1}{\rho^2}\frac{\partial^2}{\partial\phi^2}\right\}+\frac{1}{2}\rho^2\right]\hat{\sigma}_0 + g\rho\begin{pmatrix} 0 & e^{-i\phi} \\ e^{i\phi} & 0 \end{pmatrix}. \tag{4}$$

If we write the eigenfunction of the Hamiltonian as $\Psi = \Phi/\sqrt{\rho}$, the Hamiltonian for Φ becomes

$$\hat{\mathcal{H}} = \left(-\frac{1}{2}\frac{\partial^2}{\partial\rho^2}-\frac{1}{8\rho^2}+\frac{\hat{L}_z^2}{2\rho^2}+\frac{1}{2}\rho^2\right)\hat{\sigma}_0 + g\rho\begin{pmatrix} 0 & e^{-i\phi} \\ e^{i\phi} & 0 \end{pmatrix}, \tag{5}$$

where $\hat{L}_z = -i\partial/\partial\phi$. To diagonalize the potential energy matrix, the following unitary transformation is applied[12]

$$\hat{S} = \frac{1}{\sqrt{2}}\begin{pmatrix} \exp\left(-i\frac{\phi}{2}\right) & \exp\left(-i\frac{\phi}{2}\right) \\ \exp\left(i\frac{\phi}{2}\right) & -\exp\left(i\frac{\phi}{2}\right) \end{pmatrix}, \tag{6}$$

the Hamiltonian then becomes

$$\hat{S}^\dagger\hat{\mathcal{H}}\hat{S} = \left(-\frac{1}{2}\frac{\partial^2}{\partial\rho^2}+\frac{1}{2}\rho^2-\frac{1}{8\rho^2}\right)\hat{\sigma}_0+\frac{1}{2\rho^2}\left(\hat{L}_z-\frac{1}{2}\hat{\sigma}_x\right)^2 + g\rho\hat{\sigma}_z, \tag{7}$$

where

$$\hat{\sigma}_z = \begin{pmatrix} 1 & 0 \\ 0 & -1 \end{pmatrix}. \tag{8}$$

This Hamiltonian shows that the radial motion and angular motion can be separated:

$$\Phi(\rho,\phi) = \frac{1}{\sqrt{2\pi}}e^{ij\phi}\chi(\rho), \tag{9}$$

where j is the eigenvalue of the operator $\hat{J} = \hat{L}_z + \frac{1}{2}\hat{\sigma}_z$, and $j = \pm 1/2, \pm 3/2, \pm 5/2, \ldots$. The Hamiltonian for the radial motion is

$$\hat{\mathcal{H}} = \left(-\frac{1}{2}\frac{d^2}{d\rho^2}+\frac{j^2}{2\rho^2}+\frac{1}{2}\rho^2\right)\hat{\sigma}_0 - \frac{j}{2\rho^2}\hat{\sigma}_x + g\rho\hat{\sigma}_z. \tag{10}$$

This Hamiltonian is exact because we did not apply any approximation in passing from Eq. (1) to Eq. (10). This Hamiltonian yields the coupled equations

$$\begin{cases} \left(-\frac{1}{2}\frac{d^2}{d\rho^2}+\frac{j^2}{2\rho^2}+\frac{1}{2}\rho^2\right)\chi_- - |g|\rho\chi_- - \frac{j}{2\rho^2}\chi_+ = E\chi_- \\ \left(-\frac{1}{2}\frac{d^2}{d\rho^2}+\frac{j^2}{2\rho^2}+\frac{1}{2}\rho^2\right)\chi_+ + |g|\rho\chi_+ - \frac{j}{2\rho^2}\chi_- = E\chi_+ . \end{cases} \tag{11}$$

If one neglects the term $(j/(2\rho^2))\hat{\sigma}_x$ in the strong coupling limit, the coupled equations are decoupled as

$$\left(-\frac{1}{2}\frac{d^2}{d\rho^2}+\frac{j^2}{2\rho^2}+\frac{1}{2}\rho^2\right)\chi_- - |g|\rho\chi_- = E_-\chi_-, \tag{12}$$

$$\left(-\frac{1}{2}\frac{d^2}{d\rho^2}+\frac{j^2}{2\rho^2}+\frac{1}{2}\rho^2\right)\chi_+ + |g|\rho\chi_+ = E_+\chi_+, \tag{13}$$

and the Hamiltonians for the decoupled equations are

$$\mathcal{H}_\pm = -\frac{1}{2}\frac{d^2}{d\rho^2}+U_\pm(\rho), \tag{14}$$

where

$$U_\pm(\rho) = \frac{j^2}{2\rho^2}+\frac{1}{2}\rho^2 \pm |g|\rho. \tag{15}$$

The term $j^2/(2\rho^2)$ in $U_\pm(\rho)$ plays the role of the centrifugal energy. The resulting energy surfaces are shown in Figs. 1 and 2. The decoupled equation (12) is the equation for the lower sheet, and Eq. (13) for the upper sheet, respectively. These are the equations that we will discuss in the present paper.

In comparison with the so-called *Mexican hat* potential in the static Jahn-Teller problem,[12] it should be noted that the potentials diverge at the origin due to the centrifugal energy $j^2/(2\rho^2)$. This behavior of the potentials at the origin imposes a boundary condition for the wave functions: the radial

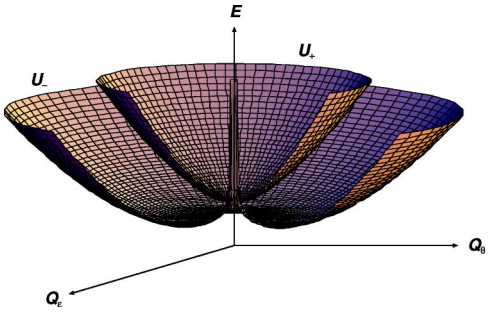

FIG. 1. Potential energy surfaces of the linear $E\otimes e$ problem including centrifugal energy. For the cross section of this potential, see Fig. 2.

part χ should be zero at the origin. According to general rules of quantum mechanics the solutions of Schrödinger equations should always obey appropriate boundary conditions, therefore we have to reconsider the previous analytical solutions for this problem.

The term neglected in Eq. (10) mixes the states of the two energy surfaces $U_{\pm}(\rho)$; to neglect this coupling is equivalent to the adiabatic approximation for the strong coupling limit. Therefore $\mathcal{H}_{\mathrm{non}}=-(j/(2\rho^2))\hat{\sigma}_x$ can be regarded as the nonadiabatic coupling.

The vibronic wave functions within this adiabatic approximation are given by[12]

$$|\pm,n,j\rangle=\psi_{\pm}^{\mathrm{ad}}(\mathbf{r})e^{ij\phi}\frac{\chi_n(\rho)}{\sqrt{2\pi\rho}}, \tag{16}$$

where $\mathbf{r}$ is the electronic coordinate, $\psi_{\pm}^{\mathrm{ad}}=\hat{S}(\psi_{\pm})$, and the total exact vibronic wave function can be written as a linear combination of these states with the same j, in which the coefficients are determined by the neglected mixing term in the Hamiltonian (10).

III. NUMERICAL SOLUTION OF THE DECOUPLED EQUATION

In this section we show the numerical solutions of the decoupled Eqs. (12) and (13) using the finite difference method[16] and compare them with the numerical solution obtained by Longuet-Higgins *et al.*[1]

We write the decoupled Eqs. (12) and (13) as

$$-\frac{1}{2}\frac{d^2\chi(\rho)}{d\rho^2}+\left(\frac{j^2}{2\rho^2}+\frac{1}{2}\rho^2-g\rho\right)\chi(\rho)=E\chi(\rho), \tag{17}$$

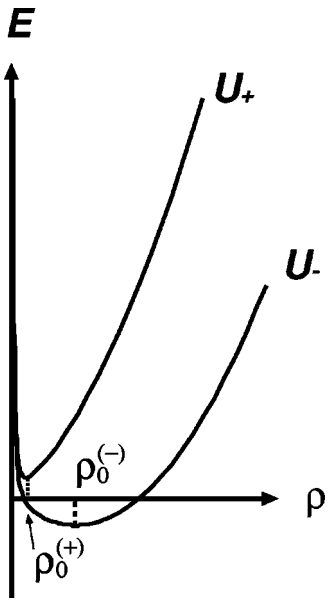

FIG. 2. Radial cross sections of the potential energy surfaces in Fig. 1.

where positive g corresponds to the equation for the lower sheet, and a negative g for the upper sheet. This is a two-point boundary problem with the boundary condition; $\chi(0)=0$ and $\chi(\infty)=0$.

We make the discretization with an increment h for this equation: $\chi_n=\chi(r_n)$ and

$$h^2\chi_n''=(\chi_{n+1}-2\chi_n+\chi_{n-1})+C_2\chi_n, \tag{18}$$

where

$$C_2=-\frac{1}{12}\delta^4+\frac{1}{90}\delta^6-\cdots, \tag{19}$$

and δ means a central difference. If the difference correction is neglected, the finite difference equation becomes

$$\chi_{n+1}+\left(-2+2Eh^2-\frac{j^2}{h^2}+2gh^3n-h^4n^2\right)\chi_n+\chi_{n-1}=0 \tag{20}$$

with the boundary condition $\chi_0=\chi(0)=0$ and $\chi_{n_{\max}+1}=\chi(r_{\mathrm{cut}})=0$, where r_{cut} is a cutoff distance. Thus $h=r_{\mathrm{cut}}/n_{\max}$. These algebraic equations yield the eigenvalue problem of the matrix form

$$\begin{pmatrix} 2gh^3 1-h^4 1^2 & 1 & 0 & \cdots \\ 1 & 2gh^3 2-h^4 2^2 & 1 & \cdots \\ 0 & 1 & 2gh^3 3-h^4 3^2 & \cdots \\ \cdots & \cdots & \cdots & \cdots \\ \cdots & 0 & 1 & 2gh^3 n_{\max}-h^4 n_{\max}^2 \end{pmatrix}\begin{pmatrix} \chi_1 \\ \chi_2 \\ \chi_3 \\ \vdots \\ \chi_{n_{\max}} \end{pmatrix}=\left(2+\frac{j^2}{h^2}-2Eh^2\right)\begin{pmatrix} \chi_1 \\ \chi_2 \\ \chi_3 \\ \vdots \\ \chi_{n_{\max}} \end{pmatrix}. \tag{21}$$

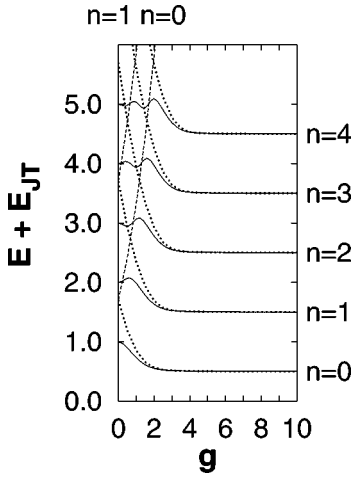

FIG. 3. Comparison of the numerical solutions for the decoupled equations of the lower sheet (12) (dotted lines) and upper sheet (13) (broken lines) for $j=1/2$ with those of the coupled equation (11) (solid lines) calculated using the $N=100$ circular oscillator basis functions after Ref. 1 in the range of $0\leqslant g\leqslant 10$, where g is dimensionless coupling constant. Energy unit is $\hbar\omega$, and $E_{\mathrm{JT}}=1/2g^2$ Jahn-Teller stabilization energy.

Figure 3 shows the calculated result of the eigenenergy for the decoupled equations for the lower and upper sheet. The energy for the lower sheet converges in the strong coupling limit, while that for the upper sheet increases monotonously. Solutions for the coupled equation are also shown. We calculated the numerical solutions of the coupled equation after Longuet-Higgins *et al.*[1] with 100 basis functions. Looking at Fig. 3, it is clear that the levels for the lower and upper sheet, calculated using the decoupled equations, do cross each other. However when the coupled equations are used, the intersections between the solutions of the two sheets become avoided, due to the nonadiabatic coupling terms. The sequence of avoided crossings gives rise to the oscillating behavior of the solutions of the coupled equations in the weak coupling region with $g<2$. Moreover, from Fig. 4, we can see that the solutions of the coupled and decoupled equation coincide up to order of $1/g^4$ in the strong coupling limit.

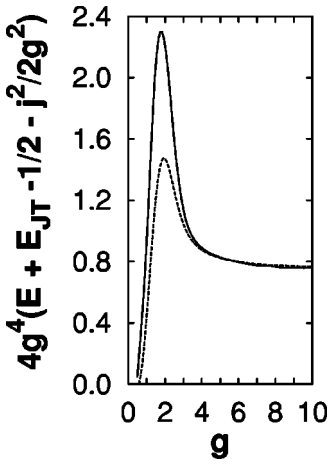

FIG. 4. Numerical solutions of the coupled equation (broken line) and decoupled equation (solid line) for the lower sheet with $j=1/2,n=0$. Energy is shown by $4g^4(E-E_{\mathrm{JT}}-\frac{1}{2}-(j^2/2g^2))$ as a function of dimensionless coupling constant g. The energy unit is $\hbar\omega$, and $E_{\mathrm{JT}}=1/2g^2$ is the Jahn-Teller stabilization energy. The solutions of the coupled and decoupled equations coincide up to power of $1/g^4$ in the strong coupling limit.

IV. ENERGY EXPRESSIONS WITHIN CRUDE APPROXIMATION

In this section, we will review the previous analytical solution within the crude approximation for the eigenstates of the linear $E\otimes e$ problem in the strong coupling limit.[12]

From Eq. (15), the trough of minima of the lower potential sheet $U_-(\rho)$ is located at

$$\rho_0^{(-)}\approx|g|+O\left(\frac{1}{|g|^3}\right), \tag{22}$$

and of the upper surface at

$$\rho_0^{(+)}\approx\left(\frac{j^2}{|g|}\right)^{1/3}+O\left(\frac{1}{|g|^{5/3}}\right). \tag{23}$$

In the strong coupling limit, the lowest eigenstates of each energy surface should be localized at the potential minimum. Therefore, expanding the potentials around the minima $\rho_0^{(-)}=|g|$ for the lower sheet and $\rho_0^{(+)}=(j^2/|g|)^{1/3}$ for the upper sheet, and keeping quadratic terms of the displacements from these minima, the Schrödinger equation for the lower and upper sheet become

$$\left(-\frac{1}{2}\frac{d^2}{dx_-^2}+\frac{1}{2}x_-^2+\frac{1}{2}g^2+\frac{j^2}{2\rho_0^{(-)2}}\right)\chi_-(x_-)=E_-\chi_-(x_-), \tag{24}$$

and

$$\left(-\frac{1}{2}\frac{d^2}{dx_+^2}+\frac{1}{2}\frac{3}{2}\left(\frac{g^2}{|j|}\right)^{2/3}x_+^2+\frac{3}{2}(j^2g^2)^{1/3}\right)\chi_+(x_+)$$
$$=E_+\chi_+(x_+), \tag{25}$$

respectively, where $x_\pm=\rho-\rho_0^{(\pm)}$. Making this harmonic approximation, we can obtain the eigenenergy and eigenfunction: for the lower sheet,

$$E_{-,nj}=\left(n+\frac{1}{2}\right)+\frac{j^2}{2g^2}-\frac{1}{2}g^2, \tag{26}$$

$$\chi_-(\rho)=e^{-(1/2)(\rho-|g|)^2}H_n(\rho-|g|), \tag{27}$$

and, for the upper sheet,

$$E_{+,nj}=\sqrt{3}\left(\frac{g^2}{|j|}\right)^{1/3}\left(n+\frac{1}{2}\right)+\frac{3}{2}(j^2g^2)^{1/3}, \tag{28}$$

$$\chi_+(\rho)=e^{-(1/2)\sqrt{3/2}(g^2/|j|)^{1/3}(\rho-(j^2/|g|)^{1/3})}$$
$$\times H_n\left(\left(\frac{3}{2}\right)^{1/4}\left(\frac{g^2}{|j|}\right)^{1/6}\left(\rho-\left(\frac{j^2}{|g|}\right)^{1/3}\right)\right). \tag{29}$$

The wave functions have finite values at the origin (see Figs. 5 and 6). This incorrect behavior of the wave function (27) and (29) prevents us from calculating the nonadiabatic coupling matrix element. We therefore have to introduce correct asymptotic behavior of these wave functions. Furthermore the coefficient of order $1/g^2$ in Eq. (26) is j^2, which is well reproduced in the numerical calculations (see Figs. 7 and 8). Note that there is no $1/g^4$ order in this expression. Therefore the crude solution is exact up to order of $1/g^2$.

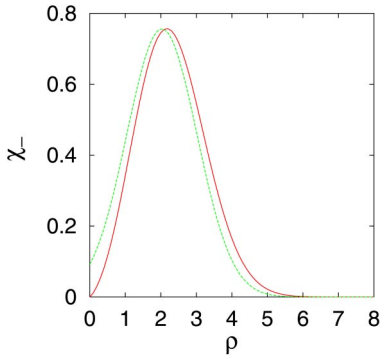

FIG. 5. Normalized wave function χ_- of the ground vibronic state $(n,j)=(0,1/2)$ for the lower potential with $g=2$. The solid line is the present result (59), and the dotted line crude one (27). The present wave function is asymmetric with respect to the maximum and the maximum is shifted. The crude wave function has a finite value at the origin, while the present wave function goes to zero.

V. ASYMPTOTIC BEHAVIOR IN THE VICINITY OF ORIGIN

Given the divergence of the centrifugal component of the potential at the origin (Figs. 1 and 2), the solution in this region is searched in the standard way[17,18]

$$\chi(\rho)=\rho^{\alpha}v(\rho), \tag{30}$$

where $v(\rho)$ is nonzero at the origin and α is a non-negative constant.

In this section, we determine the power α for both the exact coupled equations and the decoupled equations.

A. Coupled equation

If ρ goes to zero the coupled equations of the Hamiltonian (10) become

$$\begin{pmatrix} -\frac{1}{2}\frac{d^2}{d\rho^2}+\frac{j^2}{2\rho^2} & \frac{j}{2\rho^2} \\ \frac{j}{2\rho^2} & -\frac{1}{2}\frac{d^2}{d\rho^2}+\frac{j^2}{2\rho^2} \end{pmatrix}\begin{pmatrix}\chi_-\\ \chi_+\end{pmatrix}=0. \tag{31}$$

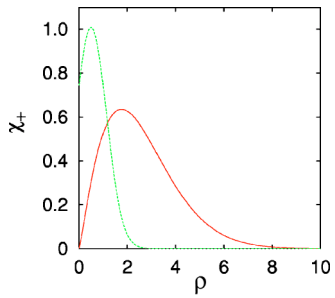

FIG. 6. Normalized wave function χ_+ of the vibronic state $(n,j)=(0,1/2)$ for the upper potential with $g=2$. The solid line is the present result (94), and the dotted line crude one (29). The present wave function is delocalized and asymmetric with respect to the maximum and the maximum is shifted (see text). The crude wave function has a finite value at the origin, while the present wave function goes to zero.

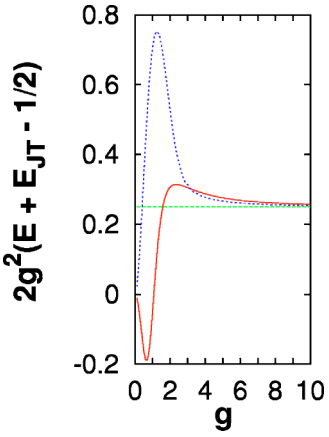

FIG. 7. Comparison of the general energy expression of Eq. (56) (solid line) with $\alpha_-=\frac{1}{2}+\sqrt{j^2+\frac{1}{4}}$ and the previous expression Eq. (26) (horizontal broken line) for the lower potential sheet, with the numerical results of the decoupled equation for the lower sheet (dotted line). $2g^2(E_{nj}-E_{\mathrm{JT}}-\frac{1}{2})$ for $(n,j)=(0,1/2)$ are shown as a function of dimensionless coupling constant g. The unit of energy is $\hbar\omega$, and $E_{\mathrm{JT}}=1/2g^2$ denotes the Jahn-Teller stabilization energy.

This matrix can be diagonalized as

$$\begin{pmatrix} -\frac{1}{2}\frac{d^2}{d\rho^2}+\frac{j^2}{2\rho^2}-\frac{j}{2\rho^2} & 0 \\ 0 & -\frac{1}{2}\frac{d^2}{d\rho^2}+\frac{j^2}{2\rho^2}+\frac{j}{2\rho^2} \end{pmatrix}\times\begin{pmatrix}\chi'_-\\ \chi'_+\end{pmatrix}=0, \tag{32}$$

where

$$\begin{pmatrix}\chi'_-\\ \chi'_+\end{pmatrix}=\frac{1}{\sqrt{2}}\begin{pmatrix}1 & 1\\ 1 & -1\end{pmatrix}\begin{pmatrix}\chi_-\\ \chi_+\end{pmatrix}. \tag{33}$$

If $\chi'_{\pm}\sim\rho^{\alpha'_{\pm}}C'_{\pm}$ in the vicinity of $\rho=0$, where $C'_{\pm}$ are nonzero constants, we have equations for α':

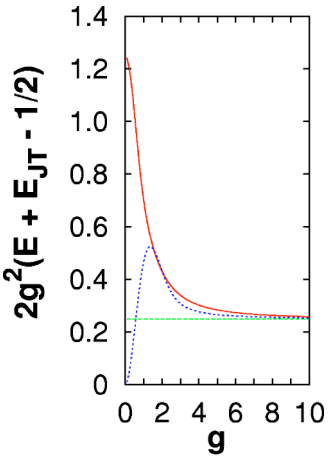

FIG. 8. Comparison of the general energy expression Eq. (56) (solid line) with $\alpha_-=|j|$ and the previous expression Eq. (26) (horizontal broken line) for the lower potential sheet, with the numerical results of the coupled equation (dotted line). $2g^2(E_{nj}-E_{\mathrm{JT}}-\frac{1}{2})$ for $(n,j)=(0,1/2)$ are shown as a function of dimensionless coupling constant g. The unit of energy is $\hbar\omega$, and $E_{\mathrm{JT}}=1/2g^2$ denotes the Jahn-Teller stabilization energy.

$$-\alpha'_{\pm}(\alpha'_{\pm}-1)+j^2\pm j=0. \tag{34}$$

The solutions are

$$\alpha'_{-}=j,1-j, \tag{35}$$

$$\alpha'_{+}=j+1,-j. \tag{36}$$

For the solution to be regular at the origin, $\alpha'_{\pm}$ should be positive. Therefore, for a positive j,

$$\alpha'_{-}=j=|j|, \tag{37}$$

$$\alpha'_{+}=j+1=|j|+1, \tag{38}$$

and, for a negative j,

$$\alpha'_{-}=1-j=|j|+1, \tag{39}$$

$$\alpha'_{+}=-j=|j|. \tag{40}$$

We pass from χ'_{-},χ'_{+} to χ_{-},χ_{+} in the vicinity of $\rho=0$:

$$\begin{cases} \chi_{-}=\dfrac{1}{\sqrt{2}}(\chi'_{-}+\chi'_{+})\sim\dfrac{1}{\sqrt{2}}(\rho^{\alpha'_{-}}C'_{-}+\rho^{\alpha'_{+}}C'_{+}) \\ \chi_{+}=\dfrac{1}{\sqrt{2}}(\chi'_{-}-\chi'_{+})\sim\dfrac{1}{\sqrt{2}}(\rho^{\alpha'_{-}}C'_{-}-\rho^{\alpha'_{+}}C'_{+}). \end{cases} \tag{41}$$

Note that $C'_{\pm}$ are nonzero constants. If we write $\chi_{\pm}\sim\rho^{\alpha_{\pm}}C_{\pm}$ in the vicinity of $\rho=0$, $\alpha_{\pm}=\min(\alpha'_{+},\alpha'_{-})$. Therefore $\alpha_{\pm}=|j|$.

B. Decoupled equation

If ρ goes to zero in the decoupled equations, they become

$$\left(-\frac{1}{2}\frac{d^2}{d\rho^2}+\frac{j^2}{2\rho^2}\right)\chi_{\pm}(\rho)=0. \tag{42}$$

If $\chi_{\pm}\sim\rho^{\alpha_{\pm}}C_{\pm}$ in the vicinity of the origin, where $C_{\pm}$ is a nonzero constant, we obtain an equation for α in the decoupled regime:

$$-\alpha_{\pm}(\alpha_{\pm}-1)+j^2=0. \tag{43}$$

Since α should be positive to obtain a physical solution,

$$\alpha_{\pm}=\tfrac{1}{2}+\sqrt{j^2+\tfrac{1}{4}}. \tag{44}$$

The fact that different α's are obtained from the coupled and decoupled equation signifies that the asymptotic behavior of the wave function around the origin is strongly influenced by the nonadiabatic coupling. This is especially true for the upper sheet even in the strong coupling limit.

Since we found that $\alpha_{-}=\alpha_{+}$ for both the coupled and decoupled equation, we will put $\alpha_{-}=\alpha_{+}=\alpha$ hereafter. Note that the crude approximation corresponds to putting $\alpha=0$.

VI. LOWER SHEET

The Schrödinger equation for the lower sheet (12) is a particular case of motion in a central field and textbook quantum mechanics[17,18] tells us that the solution should behave as ρ^{α} at the origin, where α is a constant. Though we determined α in the previous section, we keep α arbitrary in the discussion on the lower sheet in order to emphasize the fact that the energy expression in the strong coupling limit is independent of α up to the order of $1/g^2$. Let $\chi_{-}(\rho)=\rho^{\alpha}v_{-}(\rho)$, where $v_{-}(\rho)$ is assumed not to be zero at the origin; substituting it into the equation leads to

$$v''_{-}+P_{-}(\rho)v'_{-}+Q_{-}(\rho)v_{-}=0, \tag{45}$$

where

$$P_{-}(\rho)=\frac{2\alpha}{\rho}, \tag{46}$$

$$Q_{-}(\rho)=2E_{-}+\frac{\alpha^2-\alpha-j^2}{\rho^2}+2|g|\rho-\rho^2. \tag{47}$$

Since in the strong coupling limit the neighborhood of $\rho_0^{(-)}=|g|$ is the most important coordinate domain, we expand $P_{-}(\rho)$ and $Q_{-}(\rho)$ as follows:

$$P_{-}(\rho)=\frac{2\alpha}{|g|}-\frac{2\alpha}{g^2}(\rho-|g|)+\cdots, \tag{48}$$

$$\begin{aligned} Q_{-}(\rho)=&\left(2E_{-}+\frac{\alpha^2-\alpha-j^2}{g^2}+g^2\right)+\left(\frac{2\alpha-2\alpha^2+2j^2}{|g|^3}\right) \\ &\times(\rho-|g|)+\left(-1+\frac{3\alpha^2-3\alpha-3j^2}{g^4}\right)(\rho-|g|)^2 \\ &+\cdots. \end{aligned} \tag{49}$$

Let $x_{-}=\rho-|g|$, then the approximate equation becomes

$$\begin{aligned} &v''_{-}(x_{-})+(a_0^{(-)}+b_0^{(-)}x_{-})v'_{-}(x_{-})+(a_1^{(-)}+b_1^{(-)}x_{-} \\ &+c_1^{(-)}x_{-}^2)v_{-}(x_{-})=0, \end{aligned} \tag{50}$$

where

$$a_0^{(-)}=\frac{2\alpha}{|g|}, \tag{51}$$

$$b_0^{(-)}=-\frac{2\alpha}{g^2}, \tag{52}$$

$$a_1^{(-)}=2E_{-}+\frac{\alpha^2-\alpha-j^2}{g^2}+g^2, \tag{53}$$

$$b_1^{(-)}=\frac{2\alpha-2\alpha^2+2j^2}{|g|^3}, \tag{54}$$

$$c_1^{(-)}=-1+\frac{3\alpha^2-3\alpha-3j^2}{g^4}. \tag{55}$$

From Appendix A, the eigenenergy is obtained from the quantization condition as

$$\begin{aligned} E_{-}=&-\frac{\alpha^2-\alpha-j^2}{2g^2}-\frac{1}{2}g^2+\frac{b_0^{(-)}}{2}+k^{(-)} \\ &+\frac{b_0^{(-)}+4k^{(-)}}{2}n+\frac{a_0^{(-)}\tau^{(-)}}{2}-\frac{\tau^{(-)2}}{2}, \end{aligned} \tag{56}$$

where

$$k^{(-)}=\tfrac{1}{4}(-b_0^{(-)}+\sqrt{b_0^{(-)2}-4c_1^{(-)}}), \tag{57}$$

$$\tau^{(-)}=\frac{b_1^{(-)}+2a_0^{(-)}k}{b_0^{(-)}+4k^{(-)}}. \tag{58}$$

The eigenfunction is

$$\chi_-(\rho)=\rho^\alpha \exp\left(-\frac{1}{2}\zeta^{(-)2}(\rho-\lambda^{(-)})^2\right) \times\exp(\gamma^{(-)})H_n(\kappa^{(-)}(\rho-\mu^{(-)})), \tag{59}$$

where

$$\zeta^{(-)2}=2\left(k^{(-)}+\frac{b_0^{(-)}}{2}\right), \tag{60}$$

$$\lambda^{(-)}=|g|-\frac{a_0^{(-)}-\tau^{(-)}}{2k^{(-)}+b_0^{(-)}}, \tag{61}$$

$$\gamma^{(-)}=g^2\left(k^{(-)}+\frac{b_0^{(-)}}{2}\right)+\frac{(a_0^{(-)}-\tau^{(-)})^2}{4k^{(-)}+2b_0^{(-)}}, \tag{62}$$

$$\kappa^{(-)}=\sqrt{\frac{b_0^{(-)}}{2}+2k^{(-)}}, \tag{63}$$

and

$$\mu^{(-)}=|g|-\frac{a_0^{(-)}-2\tau^{(-)}}{b_0^{(-)}+4k^{(-)}}. \tag{64}$$

Since, in the strong coupling limit, these constants become

$$\zeta^{(-)}\to 1,$$
$$\kappa^{(-)}\to 1,$$
$$\mu^{(-)}\to g,$$
$$\lambda^{(-)}\to g,$$

Eq. (59) approaches the crude wave function (27) except for ρ^α.

In the strong coupling limit, we have a simplified energy expression

$$E_-=-\tfrac{1}{2}g^2+n+\tfrac{1}{2} +\frac{j^2}{2g^2}+\frac{(3\alpha-2\alpha^2+3j^2)(2n+1)}{4g^4}+O\left(\frac{1}{g^6}\right). \tag{65}$$

It should be noted that arbitrary α does not appear in the power of $1/g^2$. This is the reason why the crude energy expression[1,12] gives the correct behavior of energy up to the order of $1/g^2$ in the strong coupling region, in spite of the incorrect asymptotic behavior. Furthermore, it is important to note that the contributions of the order of $1/g^2$ originate not only from $a_1^{(-)}$ which gives the pseudorotational energy $j^2/(2g^2)$ in the crude treatment with $\alpha=0$ but also from $a_0^{(-)},b_0^{(-)},k^{(-)},\tau^{(-)}$ which are neglected in the crude approximation. In the $1/g^4$ order, we find a dependence on α. However, as we will discuss in the following section, the first-order perturbations will exactly cancel the α-dependence in the $1/g^4$ order.

Figure 5 shows a comparison between the present and crude $n=0,j=1/2$ normalized radial wave functions for the lower sheet. At the origin, the present wave functions are zero. On the other hand, the crude wave functions have finite values. The positions of the maximum of the present wave functions are shifted into larger ρ comparing to the crude ones. The asymmetric potential sheet reflects the asymmetric shapes of the wave functions. On the other hand, the crude ones have a symmetric form about the potential minimum due to the harmonic potential which is symmetric about its minimum.

Figure 7 exhibits the energy for the lower state $n=0$, $j=1/2$ using the general energy expression Eq. (56) with $\alpha=\frac{1}{2}+\sqrt{j^2+\frac{1}{4}}$. We can see that Eq. (56) reproduces the numerical solution for the decoupled equation.

If one substitutes $\alpha=|j|$ which describes the asymptotic behavior of the coupled equation into Eq. (56), it is interesting to compare it with the numerical solution of the coupled equation. Figure 8 exhibits satisfactory agreement between Eq. (56) with $\alpha=|j|$ and the numerical solution of the coupled equation. This may indicate that the asymptotic behavior ρ^α partly contains the nonadiabatic effect. Thus Eq. (56) with $\alpha=|j|$ cannot be regarded as the adiabatic energy of the decoupled equation.

VII. FIRST-ORDER CORRECTION FOR THE LOWER SHEET

In this section, the coefficients in the approximate decoupled equation for the lower sheet are assumed to be $b_1^{(-)}=0$ and $c_1^{(-)}=-1$ for simplicity. The approximate equation is written as

$$v''+\left(\frac{2\alpha}{g}-\frac{2\alpha}{g^2}(\rho-g)\right)v' +\left(2E+\frac{\alpha^2-\alpha-j^2}{g^2}+g^2-(\rho-g)^2\right)v=0. \tag{66}$$

This equation is given by the following Hamiltonian:

$$\mathcal{H}_0=-\frac{1}{2}\frac{d^2}{d\rho^2}-\left(\frac{\alpha}{g}-\frac{\alpha}{g^2}(\rho-g)\right)\frac{d}{d\rho} -\frac{1}{2}\left(\frac{\alpha^2-\alpha-j^2}{g^2}+g^2\right)+\frac{1}{2}(\rho-g)^2, \tag{67}$$

and, we regard this as the unperturbed Hamiltonian. The unperturbed energy is obtained as

$$E_{nj}^{(0)}\sim-\frac{1}{2}g^2+n+\frac{1}{2}+\frac{j^2}{2g^2}+\frac{\alpha^2}{4g^4}+O(g^{-6}). \tag{68}$$

In the v space, the normalization condition is

$$\int \rho d\rho d\phi\Psi^*\Psi=\int d\rho d\phi\Phi^*\Phi =\int d\rho\chi^*\chi=\int d\rho\rho^{2\alpha}v^*v=1. \tag{69}$$

It is found that the volume element in the v space is $\rho^{2\alpha}d\rho$. In this space, the adjoint operators are

$$\left(\frac{d^2}{d\rho^2}\right)^{\dagger}=\frac{d^2}{d\rho^2}+\frac{4\alpha}{\rho}\frac{d}{d\rho}+\frac{2\alpha(2\alpha-1)}{\rho^2}, \tag{70}$$

$$\left(\rho\frac{d}{d\rho}\right)^{\dagger}=-(2\alpha+1)-\rho\frac{d}{d\rho}, \tag{71}$$

$$\left(\frac{d}{d\rho}\right)^{\dagger}=-\frac{2\alpha}{\rho}-\frac{d}{d\rho}. \tag{72}$$

Therefore the adjoint of the unperturbed Hamiltonian (67) is obtained as

$$\mathcal{H}_0^{\dagger}=-\frac{1}{2}\frac{d^2}{d\rho^2}-\left(\frac{2\alpha}{\rho}-\frac{2\alpha}{g}+\frac{\alpha}{g^2}\rho\right)\frac{d}{d\rho}-\frac{\alpha(2\alpha-1)}{\rho^2}+\frac{4\alpha^2}{g}\cdot\frac{1}{\rho}-\frac{\alpha(2\alpha+1)}{g^2}-\frac{1}{2}\left(\frac{\alpha^2-\alpha-j^2}{g^2}+g^2\right)+\frac{1}{2}(\rho-g)^2. \tag{73}$$

It is found that the adjoint of the unperturbed Hamiltonian $\mathcal{H}_0^{\dagger}$ is different from $\mathcal{H}_0$. Therefore $\mathcal{H}_0$ is a non-Hermitian operator. Since the eigenequation of $\mathcal{H}_0^{\dagger}$ cannot be solved analytically, the same approximation which was made in the equation for $\mathcal{H}$:

$$\frac{1}{\rho}=\frac{1}{g}-\frac{1}{g^2}(\rho-g)-\cdots, \tag{74}$$

$$\frac{1}{\rho^2}=\frac{1}{g^2}+\cdots, \tag{75}$$

is applied for $\mathcal{H}_0^{\dagger}$. The approximate adjoint operator is obtained as

$$(\mathcal{H}_0^{\dagger})_{\text{approx}}=-\frac{1}{2}\frac{d^2}{d\rho^2}-\left(\frac{\alpha}{g}-\frac{\alpha}{g^2}(\rho-g)\right)\frac{d}{d\rho}-\frac{1}{2}\left(\frac{\alpha^2-\alpha-j^2}{g^2}+g^2\right)+\frac{1}{2}(\rho-g)^2. \tag{76}$$

It is found that $(\mathcal{H}_0^{\dagger})_{\text{approx}}=\mathcal{H}_0$. Since the unperturbed Hamiltonian is non-Hermitian, we have to resort to non-Hermitian perturbation theory[19] (see Appendix D).

The Hamiltonian giving the decoupled Eq. (67) in the v space is written as

$$\mathcal{H}=-\frac{1}{2}\frac{d^2}{d\rho^2}-\frac{\alpha}{\rho}\frac{d}{d\rho}+\left(\frac{j^2-\alpha^2+\alpha}{2\rho^2}+\frac{1}{2}\rho^2-g\rho\right). \tag{77}$$

Therefore the perturbation operator is defined by

$$\mathcal{V}=\mathcal{H}-\mathcal{H}_0=\left(-\frac{\alpha}{\rho}+\frac{\alpha}{g}-\frac{\alpha}{g^2}(\rho-g)\right)\frac{d}{d\rho}+\left(-\frac{\alpha^2-\alpha-j^2}{2\rho^2}+\frac{\alpha^2-\alpha-j^2}{2g^2}\right). \tag{78}$$

This operator is decomposed as

$$\mathcal{V}=\mathcal{V}_1^{(2)}+\mathcal{V}_1^{(3)}+\cdots+\mathcal{V}_0^{(1)}+\mathcal{V}_0^{(2)}+\cdots, \tag{79}$$

where

TABLE I. Comparison of the analytical expression with the numerical solutions of the decoupled and coupled equations. $4g^4(E-(-\frac{1}{2}g^2+n+\frac{1}{2}+(j^2/2g^2)))$ is calculated at large value of $g=10.0$ for $j=1/2$, $n=0$. In the analytical expression in the strong coupling limit, this is equal to $3j^2$.

j	$3j^2$	Decoupled	Coupled
1/2	0.75	0.74	0.77
3/2	6.75	6.78	6.80
5/2	18.75	18.37	18.36
7/2	36.75	34.45	34.42
9/2	60.75	53.53	53.44

$$\mathcal{V}_1^{(2)}=-\frac{\alpha}{g^3}(\rho-g)^2\frac{d}{d\rho}, \tag{80}$$

$$\mathcal{V}_1^{(3)}=\frac{\alpha}{g^4}(\rho-g)^3\frac{d}{d\rho}, \tag{81}$$

$$\mathcal{V}_0^{(1)}=\frac{\alpha^2-\alpha-j^2}{g^3}(\rho-g), \tag{82}$$

$$\mathcal{V}_0^{(2)}=-\frac{3(\alpha^2-\alpha-j^2)}{2g^4}(\rho-g)^2. \tag{83}$$

From Appendices B and C, we obtain the first energy correction up to $1/g^4$ as

$$E_{0j}^{(0)}+E_{0j}^{(1)}\sim-\frac{1}{2}g^2+n+\frac{1}{2}+\frac{j^2}{2g^2}+\frac{3j^2}{4g^4}. \tag{84}$$

Table I shows the coefficient of $1/g^4$ order obtained from the numerical calculations of the decoupled and coupled equation, and the present analytical expression $3j^2$. We find that agreement between the corrected energy expression (84) and the numerical results is quite good.

VIII. UPPER SHEET

In this section, α is put to be equal to $\frac{1}{2}+\sqrt{j^2+\frac{1}{4}}$. The equation for the upper sheet is

$$v_+''+\frac{2\left(\frac{1}{2}+\sqrt{j^2+\frac{1}{4}}\right)}{\rho}v_+'+(2E_+-2|g|\rho-\rho^2)v_+=0. \tag{85}$$

In the second term of the equation, if $1/\rho$ is expanded around $\rho_0^{(+)}=(j^2/g)^{1/3}$, the approximate equation can be written as

$$v_+''+(a_0^{(+)}+b_0^{(+)}(\rho-\rho_0^{(+)}))v_+'+(a_1^{(+)}+b_1^{(+)}(\rho-\rho_0^{(+)})+c_1^{(+)}(\rho-\rho_0^{(+)})^2)v_+=0, \tag{86}$$

where

$$a_0^{(+)}=\frac{2\alpha}{\rho_0}=\frac{1+\sqrt{1+4j^2}}{j^{2/3}}g^{1/3}, \tag{87}$$

$$b_0^{(+)}=-\frac{2\alpha}{\rho_0^{(+)2}}=-\frac{1+\sqrt{1+4j^2}}{j^{4/3}}g^{2/3}, \tag{88}$$

$$a_1^{(+)}=2E-2g\rho_0^{(+)}-\rho_0^{(+)2}=2E_+-2j^{2/3}g^{2/3}-j^{4/3}g^{-(2/3)}, \tag{89}$$

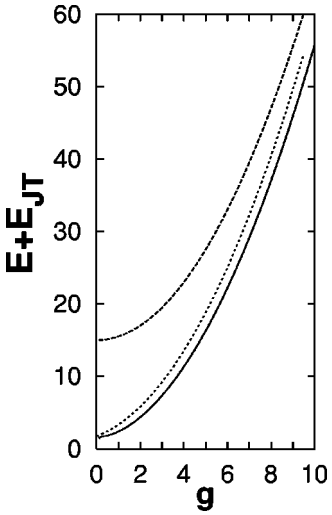

FIG. 9. Energy for upper sheet E_+ using the present expression (92) (solid line) and within the crude approximation (28) (broken line), and the numerical solution $E_{\rm up}$ (dotted line) for the decoupled equation for the upper sheet with $j=1/2$, $n=0$. The energies are shown by $E+E_{\rm JT}$ as a function of dimensionless coupling constant g, where $E_{\rm JT}=1/2g^2$ is the Jahn-Teller stabilization energy.

$$b_1^{(+)}=-2g-2\rho_0^{(+)}=-2g-2j^{2/3}g^{-(1/3)}, \tag{90}$$

$$c_1^{(+)}=-1. \tag{91}$$

The eigenenergy is obtained as

$$E_+=j^{2/3}g^{2/3}+\frac{1}{2}j^{4/3}g^{-(2/3)}+\frac{b_0^{(+)}}{2}+k^{(+)} + \frac{b_0^{(+)}+4k^{(+)}}{2}n+\frac{a_0^{(+)}\tau^{(+)}}{2}-\frac{\tau^{(+)2}}{2}. \tag{92}$$

In the strong coupling limit the simplified energy expression has the form as

$$E_+\sim\left(3j^2-1+\alpha\left(n+\frac{1}{2}\right)\right)\left(\frac{g}{j^2}\right)^{2/3}+O(|g|^{-(2/3)}), \tag{93}$$

where $\alpha=\frac{1}{2}+\sqrt{j^2+\frac{1}{4}}$. This energy expression is different from that of the crude approximation.

Figure 9 shows the energy for the upper sheet calculated by the energy expression Eq. (92) and the numerical calculation of the decoupled equation using the finite difference method. The agreement of the present results with the numerical result is clearly improved.

In the energy expression, we found that an effect of α appears in the lowest order of g. This means that the energy is strongly influenced by the existence of ρ^α. This will be clearly understood from the eigenfunction as discussed below. The eigenfunction for the upper sheet can be written as

$$\chi_+(\rho)=\rho^\alpha\exp[-\tfrac{1}{2}\zeta^{(+)2}(\rho-\lambda^{(+)})^2] \times\exp(\gamma^{(+)})H_n(\kappa^{(+)}(\rho-\mu^{(+)}), \tag{94}$$

where

$$k^{(+)}=\tfrac{1}{4}(-b_0^{(+)}+\sqrt{b_0^{(+)2}-4c_1^{(+)}}), \tag{95}$$

$$\tau^{(+)}=\frac{b_1^{(+)}+2a_0^{(+)}k}{b_0^{(+)}+4k^{(+)}}, \tag{96}$$

$$\zeta^{(+)}=\sqrt{2k^{(+)}+b_0^{(+)}}, \tag{97}$$

$$\lambda^{(+)}=\rho_0^{(+)}-\frac{a_0^{(+)}}{2k^{(+)}+b_0^{(+)}}, \tag{98}$$

$$\gamma^{(+)}=\frac{a_0^{(+)2}}{4k^{(+)}+2b_0^{(+)}}, \tag{99}$$

$$\kappa^{(+)}=\sqrt{\frac{b_0^{(+)}+4k^{(+)}}{2}}, \tag{100}$$

$$\mu^{(+)}=\rho_0^{(+)}-\frac{a_0^{(+)}-2\tau^{(+)}}{\sqrt{2(b_0^{(+)}+4k^{(+)})}}. \tag{101}$$

The wave function in the crude approximation is essentially that of the harmonic potential. On the other hand, the present function for the upper sheet is far from the wave function of the harmonic potential; (1) the position of the extrema are displaced towards larger ρ as compared to the harmonic wave function; (2) the present wave function has smaller curvature than expected for the harmonic wave function. In other words, the wave function is more delocalized than the harmonic wave function. The curvature depends on $\zeta^{(+)}$. In the strong coupling limit,

$$\zeta^{(+)}=\sqrt{k^{(+)}+\frac{b_0^{(+)}}{2}}\sim\frac{2j^4}{\alpha}g^{-(1/3)}, \tag{102}$$

where $\alpha=\frac{1}{2}+\sqrt{j^2+\frac{1}{4}}$. Since the highest orders in $k^{(+)}$ and $b_0^{(+)}/2$ cancel, $\zeta^{(+)}$ decreases as g increases. In other words, the curvature at large ρ becomes small as the coupling increases. Figure 6 shows a comparison between the present and crude normalized eigenfunctions for the upper potential sheet. At the origin, moreover, the present wave functions are zero, while the crude wave function has a finite value.

Though the upper energy expression is better than that of the crude approximation, there is still a discrepancy. It is found that a $g^{2/3}$ contribution is still missing in the present energy expression.

IX. NONADIABATIC COUPLING

The nonadiabatic coupling matrix element is written as

$$\frac{\langle\chi_{nj}^-|\dfrac{j}{2\rho^2}|\chi_{mj}^+\rangle}{\sqrt{\langle\chi_{nj}^-|\chi_{nj}^-\rangle}\sqrt{\langle\chi_{mj}^+|\chi_{mj}^+\rangle}}=\frac{j}{2}\frac{I_{{\rm non},j}^{(n,m)}}{\sqrt{\langle\chi_{nj}^-|\chi_{nj}^-\rangle}\sqrt{\langle\chi_{mj}^+|\chi_{mj}^+\rangle}}, \tag{103}$$

where

$$I_{{\rm non},j}^{(n,m)}=\int_0^\infty\rho d\rho\chi_{nj}^-(\rho)\frac{1}{\rho^2}\chi_{mj}^+(\rho). \tag{104}$$

From Appendix B, the integral $I_{{\rm non},j}^{(n,m)}$ is obtained as

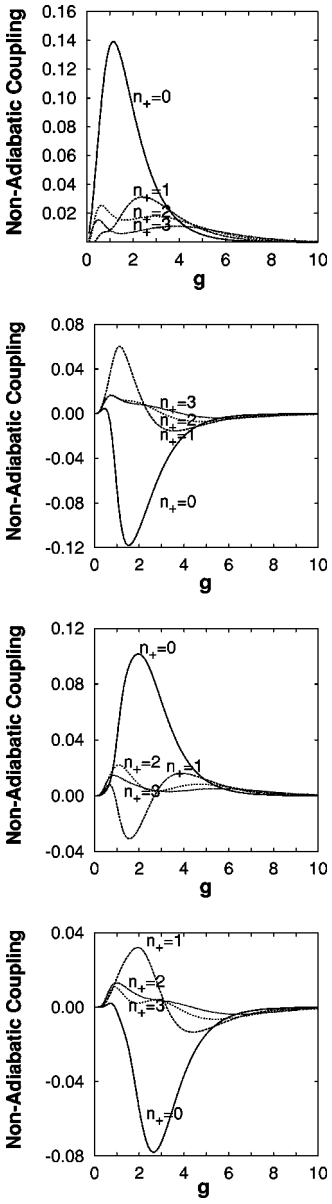

FIG. 10. Nonadiabatic coupling integrals as a function of g between the upper $j=1/2$ states and (a) the lower $n_-=0$, $j=1/2$; (b) the lower $n_-=1$, $j=1/2$; (c) the lower $n_-=2$, $j=1/2$; (d) the lower $n_-=3$, $j=1/2$.

TABLE III. Calculated nonadiabatic coupling integral for the lower $n_-=1$ state and the upper $n_+=0,1,2,3$ states.

g	$n_+=0$	$n_+=1$	$n_+=2$	$n_+=3$
1.0	−0.06612	0.05834	0.01459	0.01435
2.0	−0.10316	0.01840	0.00994	0.00839
3.0	−0.05099	−0.01231	0.00070	0.00467
4.0	−0.02003	−0.01438	−0.00592	−0.00026
5.0	−0.00742	−0.00912	−0.00678	−0.00332
6.0	−0.00268	−0.00469	−0.00501	−0.00390
7.0	−0.00094	−0.00215	−0.00299	−0.00310
8.0	−0.00032	−0.00090	−0.00156	−0.00200
9.0	−0.00010	−0.00035	−0.00074	−0.00108
10.0	−0.00003	−0.00013	−0.00039	−0.00033

$$I_{\mathrm{non},j}^{(n,m)}=\exp(\gamma^{(-)}+\gamma^{(+)}+\gamma_0)\frac{e^{-\zeta_0^2\lambda_0^2}}{2}\sum_{l=0}^{n}\sum_{k=0}^{m}\binom{n}{l}\binom{m}{k}$$
$$\times(2\kappa^{(-)})^{n-l}(2\kappa^{(+)})^{m-k}$$
$$\times H_l(-\kappa^{(-)}\mu^{(-)})H_k(-\kappa^{(+)}\mu^{(+)})$$
$$\times\zeta_0^{-1-2\alpha+2-n-m+l+k}$$
$$\times M(2\alpha-2+n+m-l-k,\zeta_0,\lambda_0), \tag{105}$$

where

$$\zeta_0=\sqrt{\frac{\zeta^{(-)2}+\zeta^{(+)2}}{2}}, \tag{106}$$

$$\lambda_0=\frac{\zeta^{(-)2}\lambda^{(-)}+\zeta^{(+)2}\lambda^{(+)}}{\zeta^{(-)2}+\zeta^{(+)2}}, \tag{107}$$

$$\gamma_0=-\frac{1}{2}\frac{\zeta^{(-)2}\zeta^{(+)2}(\lambda^{(+)}-\lambda^{(-)})^2}{\zeta^{(-)2}+\zeta^{(+)2}}. \tag{108}$$

Note that the matrix element between states with different j vanishes.

Figure 10 and Tables II–IV show the nonadiabatic coupling integrals calculated using Eq. (105). It is found from these Figures that some extrema exist in the weak coupling region where the avoided crossing occurs. and the nonadiabatic coupling rapidly decays as the vibronic coupling in-

TABLE II. Calculated nonadiabatic coupling integral for the lower $n_-=0$ state and the upper $n_+=0,1,2,3$ states.

g	$n_+=0$	$n_+=1$	$n_+=2$	$n_+=3$
1.0	0.13622	0.00818	0.02024	0.00830
2.0	0.09256	0.02891	0.01593	0.00698
3.0	0.03853	0.02828	0.01786	0.01006
4.0	0.01442	0.01757	0.01514	0.01103
5.0	0.00523	0.00901	0.01021	0.00940
6.0	0.00185	0.00413	0.00589	0.00665
7.0	0.00063	0.00175	0.00302	0.00407
8.0	0.00021	0.00069	0.00142	0.00222
9.0	0.00007	0.00026	0.00062	0.00106
10.0	0.00002	0.00009	0.00031	0.00030

TABLE IV. Calculated nonadiabatic coupling integral for the lower $n_-=3$ state and the upper $n_+=0,1,2,3$ states.

g	$n_+=0$	$n_+=1$	$n_+=2$	$n_+=3$
1.0	−0.00218	0.01553	0.01058	0.01311
2.0	−0.05478	0.03208	0.00229	0.00619
3.0	−0.07231	0.00653	0.00344	0.00356
4.0	−0.03672	−0.01226	−0.00221	0.00121
5.0	−0.01444	−0.01188	−0.00613	−0.00194
6.0	−0.00535	−0.00717	−0.00595	−0.00364
7.0	−0.00192	−0.00359	−0.00413	−0.00357
8.0	−0.00067	−0.00161	−0.00237	−0.00263
9.0	−0.00023	−0.00066	−0.00122	−0.00156
10.0	−0.00007	−0.00026	−0.00068	−0.00051

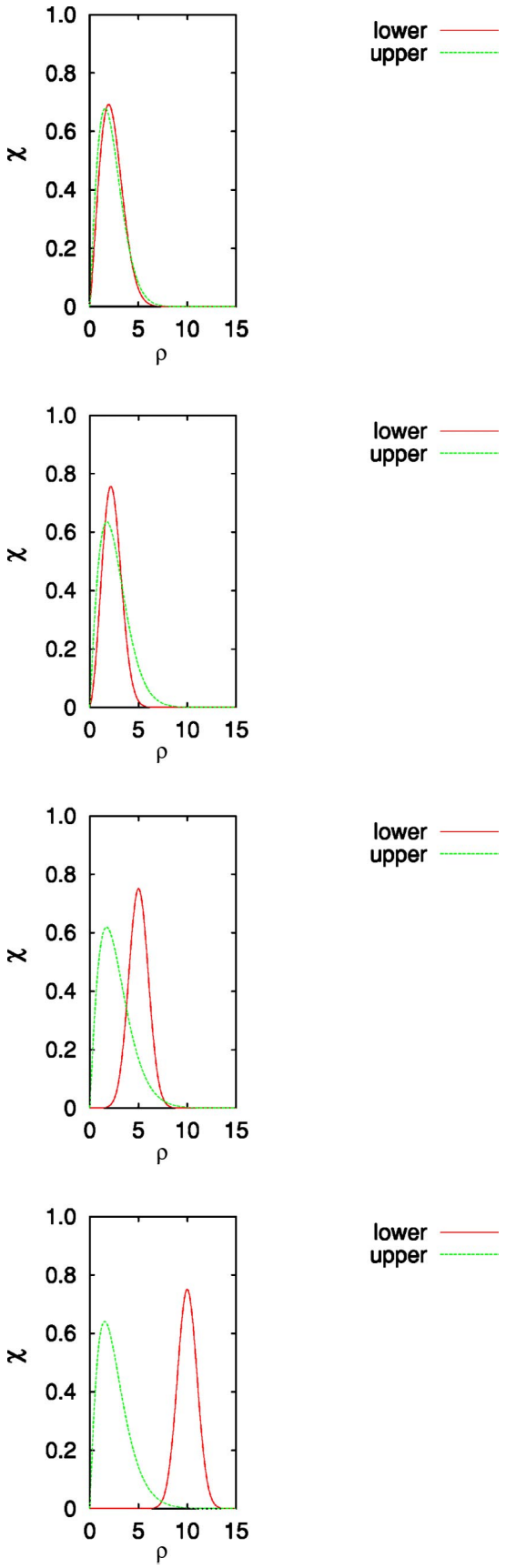

FIG. 11. Overlap between the wave functions of the lower and upper sheet with $n=0$, and $j=1/2$. (a) $g=1.0$, (b) $g=2.0$, (c) $g=5.0$, (d) $g=10.0$. As the vibronic coupling increases, the maximum of the upper function slowly approaches to the origin, while that of the lower sheet follows the minimum point of the lower potential, $\rho_0 \sim g$.

creases. In other words, the nonadiabaticity is negligibly small in the strong coupling region. That is the reason why the numerical solutions of the coupled and decoupled equations coincided in the strong coupling region.

Figure 11 shows the overlap between the wave functions of the lower and upper sheet with $n=0$, and $j=1/2$. (a) $g=1.0$, (b) $g=2.0$, (c) $g=5.0$, (d) $g=10.0$. As the vibronic coupling increases, the maximum of the upper function slowly approaches the origin, while that of the lower sheet follows the minimum point of the lower potential, $\rho_0^{(-)} \sim g$. Since the overlap is the largest for $g \approx 2.0$, the maximum of the nonadiabatic coupling lies around $g \approx 2.0$ as shown in Fig. 10.

From perturbational point of view, energy correction due to the nonadiabatic coupling is estimated to be of order of $1/g^6$, since the nonadiabatic coupling integral is of order of $1/g^2$ and the energy difference between upper and lower sheet is of order of g^2.

X. CONCLUSION

We obtained an approximate analytical solution with the correct boundary conditions for the $E\otimes e$ dynamic Jahn-Teller problem in the strong coupling limit. Compared with the previous solutions, the eigenfunctions contain factors $\rho^{|j|}$ for the coupled equation and $\rho^{1/2+\sqrt{j^2+1/4}}$ for the decoupled equation. As a results the solutions for the upper sheet look entirely different from those obtained by Slonczewski.[20]

The levels for the lower and upper sheet, numerically calculated using the decoupled equations, do cross each other. However when the coupled equations are used, the intersections between the solutions of the two sheets become avoided, due to the nonadiabatic coupling terms. The sequence of avoided crossings gives rise to the oscillating behavior of the solutions of the coupled equations in the weak coupling region with $g<2$.

The vibronic energy spectra obtained show better agreement with a numerical calculation for the coupled and decoupled equations than the crude ones in the wide range of g. For the ground vibronic state, the agreement is good up to $g \approx 1.5$ with $\alpha=|j|$.

The first order perturbation yields energy correction of the order of g^{-4} in the strong coupling limit with $\alpha=1/2+\sqrt{j^2+1/4}$. Moreover the asymptotic behavior of the lower wave function does not influence the corrected energy up to the power of $1/g^4$.

Due to the correct boundary condition, we evaluate the nonadiabatic coupling between vibronic states of the lower and upper potential sheets. It is found that the corresponding matrix elements decrease very fast with the coupling constant. Moreover the order of energy correction due to the nonadiabatic coupling is estimated to be of order of $1/g^6$.

ACKNOWLEDGMENTS

T.S. would like to thank the research fund for study abroad from Ministry of Education, Culture, Science, and Technology of Japan. Numerical calculation was partly per-

formed in the Supercomputer Laboratory of Kyoto University. Research in Leuven was supported by the Belgian Government and the FWO-Vlaanderen.

APPENDIX A: SOLUTION OF THE DIFFERENTIAL EQUATION

The equation to be solved has a form:

$$y''(x)+(a_0+b_0x)y'(x)+(a_1+b_1x+c_1x^2)y(x)=0. \quad \text{(A1)}$$

Putting $y(x)=u(x)\exp(kx^2)$ leads to

$$u''+(a_0+(b_0+4k)x)u'+((a_1+2k)+(b_1+2a_0k)x)u=0, \quad \text{(A2)}$$

where k satisfies

$$4k^2+2b_0k+c_1=0. \quad \text{(A3)}$$

Since k should be positive, k is

$$k=\tfrac{1}{4}(-b_0+\sqrt{b_0^2-4c_1}). \quad \text{(A4)}$$

Let $u(x)=v(x)\exp(-\tau x)$,

$$v''+(a_0-2\tau+(b_0+4k)x)v'+(\tau^2-a_0\tau+a_1+2k)v=0, \quad \text{(A5)}$$

where $\tau=(b_1+2a_0k)/(b_0+4k)$.

Putting $z=a_0-2\tau+(b_0+4k)x$ and $v(x)=w(z)$ leads to

$$w''(z)+\frac{1}{b_0+4k}zw'(z)+\frac{1}{(b_0+4k)^2}\times(\tau^2-a_0\tau+a_1+2k)w(z)=0. \quad \text{(A6)}$$

Let $t=-[1/(2(b_0+4k))]z^2$ and $F(t)=w(z)$, and the equation becomes

$$tF''(t)+\left(\frac{1}{2}-t\right)F'(t)-\frac{1}{2(b_0+4k)}\times(\tau^2-a_0\tau+a_1+4k)F(t)=0. \quad \text{(A7)}$$

This is the Kummer equation.

The general solution of the equation is a linear combination of the two linear independent ones:

$$F_1(t)={}_1F_1(a,\tfrac{1}{2};t), \quad \text{(A8)}$$

$$F_2(t)=t^{1/2}\ {}_1F_1(a+\tfrac{1}{2},\tfrac{3}{2};t), \quad \text{(A9)}$$

where ${}_1F_1(a,c;t)$ is a confluent hypergeometric function, and a is defined by

$$a=-\frac{1}{2(b_0+4k)}(\tau^2-a_0\tau+(a_1+4k)), \quad \text{(A10)}$$

$$w_1(z)=F_1(t) \quad \text{(A11)}$$

$$=\exp\left(-\frac{z^2}{2(b_0+4k)}\right)\times H_{2n_1}\left(\sqrt{\frac{1}{2(b_0+4k)}}z\right)\frac{(-1)^{n_1}}{(2n_1-1)!!}. \quad \text{(A12)}$$

On the other hand,

$$w_2(z)=F_2(t) \quad \text{(A13)}$$

$$=\exp\left(-\frac{z^2}{2(b_0+4k)}\right)H_{2n_2+1}\left(\sqrt{\frac{1}{2(b_0+4k)}}z\right)\times\sqrt{-\frac{1}{2(b_0+4k)}}\frac{(-1)^{n_2}}{(2n_2+1)!!}. \quad \text{(A14)}$$

From the condition for the solutions to be regular at origin,

$$\begin{cases}2a-1=2n_1\\2a-1=2n_2+1.\end{cases} \quad \text{(A15)}$$

Therefore the two solutions and the conditions can be written as a single expression:

$$\exp\left(-\frac{z^2}{2(b_0+4k)}\right)H_n\left(\sqrt{\frac{1}{2(b_0+4k)}}z\right) \quad \text{(A16)}$$

and

$$2a-1=n. \quad \text{(A17)}$$

Finally, apart from a constant, the solution is

$$y(x)=\exp\left(-\left(k+\frac{b_0}{2}\right)x^2-a_0x\right)\times H_n\left(\sqrt{\frac{(b_0+4k)}{2}}\left(x+\frac{a_0-2\tau}{\sqrt{2(b_0+4k)}}\right)\right), \quad \text{(A18)}$$

and the quantization condition is

$$\frac{a_1}{2}=\left(\frac{b_0+4k}{2}\right)n+\frac{b_0}{2}+k+\frac{a_0\tau}{2}-\frac{\tau^2}{2}. \quad \text{(A19)}$$

APPENDIX B: INTEGRAL $I_a^{(n,m)}$

$$I_a^{(n,m)}=e^{2\gamma}\int_0^\infty d\rho\rho^a\exp(-\zeta^2(\rho-\lambda)^2)H_n(\kappa_1(\rho-\mu_1))\times H_m(\kappa_2(\rho-\mu_2)). \quad \text{(B1)}$$

The Hermite polynomial $H_n(x)$ can be written in an integral representation as

$$H_n(x)=\sqrt{\frac{2^{n-1}}{\pi}}\int_{-\infty}^{\infty}e^{-(t^2/2)}(\sqrt{2}x+it)^n dt. \quad \text{(B2)}$$

Substituting this representation into the integral yields

$$I_a^{(n,m)}=e^{2\gamma}\frac{e^{-\zeta^2\lambda^2}}{2}\sum_{l=0}^{n}\sum_{k=0}^{m}\binom{n}{l}\binom{m}{k}(2\kappa_1)^{n-l}(2\kappa_2)^{m-k}\times H_l(-\kappa_1\mu_1)H_k(-\kappa_2\mu_2)\zeta^{-1-a-m-n+l+k}\times M(a+m+n-l-k,\zeta,\lambda), \quad \text{(B3)}$$

where

$$M(a,\zeta,\lambda)=2\zeta\lambda\Gamma\left(1+\frac{a}{2}\right){}_1F_1\left(1+\frac{a}{2},\frac{3}{2};\zeta^2\lambda^2\right)+\Gamma\left(\frac{1+a}{2}\right){}_1F_1\left(\frac{1+a}{2},\frac{1}{2};\zeta^2\lambda^2\right). \quad \text{(B4)}$$

APPENDIX C: ASYMPTOTIC BEHAVIOR OF $I_a^{(n,m)}$

Since the asymptotic behavior of the confluent hypergeometric function is[17]

$$ {}_1F_1(a,c;z)\sim\frac{\Gamma(c)}{\Gamma(c-a)}(-z)^{-a}G(a,a-c+1,-z) + \frac{\Gamma(c)}{\Gamma(a)}e^z(z)^{a-c}G(c-a,1-a,z), \tag{C1}$$

where G is an asymptotic series;

$$ G(a,b,z)=1+\frac{ab}{1!\,z}+\frac{a(a+1)b(b+1)}{2!z^2}+\cdots+ \tag{C2}$$

the asymptotic behavior of $M(a,\zeta,\lambda)$ is

$$ M(a,\zeta,\lambda)\sim 2\sqrt{\pi}e^{\zeta^2\lambda^2}\zeta^a\lambda^a G\left(\frac{1}{2}-\frac{a}{2},-\frac{a}{2},\zeta^2\lambda^2\right). \tag{C3}$$

Therefore

$$ I_a^{(n,m)}\sim\sqrt{\pi}e^{2\gamma}\zeta^{-1}\sum_{l=0}^{n}\sum_{k=0}^{m}\binom{n}{l}\binom{m}{k}(2\kappa)^{n+m-l-k} \times H_l(-\kappa\mu)H_k(-\kappa\mu)\lambda^{a+n+m-l-k} \times G\left(\frac{1}{2}-\frac{a+n+m-l-k}{2},-\frac{a+n+m-l-k}{2},\zeta^2\lambda^2\right). \tag{C4}$$

For $n=0$ and $m=0$,

$$ I_a^{(0,0)}\sim\lambda^a G\left(\frac{1}{2}-\frac{a}{2},-\frac{a}{2},\zeta^2\lambda^2\right). \tag{C5}$$

APPENDIX D: NON-HERMITIAN PERTURBATION THEORY

The Hamiltonian $\mathcal{H}$ is decomposed as $\mathcal{H}=\mathcal{H}_0+\epsilon\mathcal{V}$, where ϵ is a small parameter. We assume the unperturbed Hamiltonian $\mathcal{H}_0$ and the perturbation $\mathcal{V}$ can be a non-Hermitian operator. The eigenequations of $\mathcal{H}_0$ and $\mathcal{H}$ are written as

$$ \mathcal{H}_0|e_0\rangle=a_0|e_0\rangle \tag{D1}$$

and

$$ \mathcal{H}|x\rangle=\lambda|x\rangle, \tag{D2}$$

where λ and $|x\rangle$ are expanded as

$$ \lambda=a_0+\epsilon\lambda_1+\cdots, $$

$$ |x\rangle=|e_0\rangle+\epsilon|x_1\rangle+\cdots. \tag{D3}$$

Since $\mathcal{H}_0^\dagger\neq\mathcal{H}_0$, the Hermite conjugate operator $\mathcal{H}_0^\dagger$ has different eigenvectors from $\mathcal{H}_0$:

$$ \mathcal{H}_0^\dagger|f_0\rangle=a_0|f_0\rangle, \tag{D4}$$

but the eigenvalues are the same. The adjoint of this equation can be obtained as

$$ \langle f_0|\mathcal{H}_0=a_0\langle f_0|. \tag{D5}$$

Substituting Eq. (D3) into Eq. (D2) and taking the first-order of ϵ, we obtain

$$ (\mathcal{H}_0-a_0)|x\rangle=\lambda_1|e_0\rangle-\mathcal{V}|e_0\rangle. \tag{D6}$$

Multiplying $\langle f_0|$ from the left side, and using Eq. (D5), we can obtain the first-order energy correction:

$$ \lambda_1=\frac{\langle f_0|\mathcal{V}|e_0\rangle}{\langle f_0|e_0\rangle}. \tag{D7}$$

In the present problem, since Eq. (D5) cannot be solved analytically, we adopted the approximate Hamiltonian $(\mathcal{H}_0^\dagger)_{\text{approx}}$, which is equal to $\mathcal{H}_0$. The eigenequation is written as

$$ (\mathcal{H}_0^\dagger)_{\text{approx}}|f_0'\rangle=\mathcal{H}_0|e_0\rangle=a_0|e_0\rangle. \tag{D8}$$

Since

$$ \mathcal{H}_0^\dagger=(\mathcal{H}_0^\dagger)_{\text{approx}}+\frac{1}{g^2}\mathcal{A}_1+\frac{1}{g^3}\mathcal{A}_2+\cdots, \tag{D9}$$

$|f_0\rangle$ can be expanded as a series of g around $g\to\infty$,

$$ |f_0\rangle=|f_0'\rangle+\frac{1}{g^2}|y_1\rangle+\cdots, \tag{D10}$$

where $|y_1\rangle$ is a coefficient of $1/g^2$. Substituting Eq. (D10) into Eq. (D7), we obtain

$$ \lambda_1=\frac{\langle f_0'|\mathcal{V}|e_0\rangle}{\langle f_0'|e_0\rangle}+O(g^{-6}). \tag{D11}$$

Therefore we can employ

$$ \lambda_1=\frac{\langle e_0|\mathcal{V}|e_0\rangle}{\langle e_0|e_0\rangle} \tag{D12}$$

to obtain the energy correction up to order of $1/g^4$.

[1] H. Longuet-Higgins, U. Öpik, M. Pryce, and R. Sack, Proc. R. Soc. London, Ser. A **244**, 1 (1958).
[2] M. Child and H. Longuet-Higgins, Philos. Trans. R. Soc. London, Ser. A **254**, 259 (1961).
[3] S. Muramatsu and N. Sakamoto, J. Phys. Soc. Jpn. **44**, 1640 (1978).
[4] M. O. S. Evangelou, J. Phys. C **13**, 611 (1980).
[5] B. Judd, J. Phys. C **12**, 1685 (1979).
[6] H. G. Reik, M. Stülze, and M. Doucha, J. Phys. A **20**, 6327 (1987).
[7] M. Szopa and A. Ceulemans, J. Phys. A **30**, 1295 (1997).
[8] A. Thiel and H. Köppel, J. Chem. Phys. **110**, 9371 (1999).
[9] K. Bosnick, Chem. Phys. Lett. **317**, 524 (2000).
[10] J. Dunn and M. Eccles, Phys. Rev. B **64**, 195104 (2001).
[11] I. Bersuker and B. Vekhter, Fiz. Tverd. Tela (Leningrad) **9**, 2652 (1967).
[12] I. Bersuker and V. Polinger, *Vibronic Interactions in Molecules and Crystals* (Springer-Verlag, Berlin, 1989).
[13] C. Mead, J. Chem. Phys. **78**, 807 (1983).
[14] A. Varandas and Z. Xu, Chem. Phys. **259**, 173 (2000).
[15] A. Varandas and Z. Xu, Chem. Phys. Lett. **316**, 248 (2000).
[16] L. Fox, *The Numerical Solution of Two-Point Boundary Problems in Ordinary Differential Equations* (Dover, New York, 1990).
[17] L. Landau, E. Lifshitz, and J. Sykes, *Quantum Mechanics: Nonrelativistic Theory* (Pergamon, Oxford, 1965).
[18] S. Flügge, *Practical Quantum Mechanics* (Springer, Berlin, 1974).
[19] E. Hinch, *Perturbation Methods* (Cambridge University Press, Cambridge, 1991).
[20] J. Slonczewski, Phys. Rev. **131**, 1596 (1963).